

JGR Atmospheres

RESEARCH ARTICLE

10.1029/2018JD030062

This article is a companion to Ware et al. (2019), <https://doi.org/10.1029/2018JD029224>.

Key Points:

- We detected and spatio-temporally resolved major methane flux anomalies in the Los Angeles Megacity Domain
- We characterized sub-weekly scale variability in methane fluxes of South Coast Air Basin
- We evaluated the impact of the loss of observational sensitivity on methane flux estimates

Correspondence to:

V. Yadav,
vineet.yadav@jpl.nasa.gov

Citation:

Yadav, V., Duren, R., Mueller, K., Verhulst, K. R., Nehr Korn, T., Kim, J., et al. (2019). Spatio-temporally resolved methane fluxes from the Los Angeles megacity. *Journal of Geophysical Research: Atmospheres*, 124, 5131–5148. <https://doi.org/10.1029/2018JD030062>

Received 1 DEC 2018





Accepted 29 MAR 2019

Accepted article online 8 APR 2019

Published online 13 MAY 2019

Published 2019. This article is a U.S. Government work and is in the public domain in the USA.

Spatio-temporally Resolved Methane Fluxes From the Los Angeles Megacity

Vineet Yadav¹ , Riley Duren¹ , Kim Mueller² , Kristal R. Verhulst¹ , Thomas Nehr Korn³ , Jooil Kim⁴ , Ray F. Weiss⁴ , Ralph Keeling⁴ , Stanley Sander¹ , Marc L. Fischer⁵, Sally Newman^{6,7} , Matthias Falk⁸ , Toshihiro Kuwayama⁸, Francesca Hopkins⁹ , Talha Rafiq⁹, James Whetstone², and Charles Miller¹ 

¹Jet Propulsion Laboratory, California Institute of Technology, Pasadena, CA, USA, ²National Institute of Standards and Technology, Gaithersburg, MD, USA, ³Atmospheric and Environmental Research, Lexington, MA, USA, ⁴Scripps Institution of Oceanography, University of California, San Diego, La Jolla, CA, USA, ⁵Lawrence Berkeley National Laboratory, Berkeley, CA, USA, ⁶California Institute of Technology, Pasadena, CA, USA, ⁷Now at Bay Area Air Quality Management District, San Francisco, CA, USA, ⁸California Air Resources Board, Sacramento, CA, USA, ⁹University of California Riverside, Riverside, CA, USA

Abstract We combine sustained observations from a network of atmospheric monitoring stations with inverse modeling to uniquely obtain spatiotemporal (3-km, 4-day) estimates of methane emissions from the Los Angeles megacity and the broader South Coast Air Basin for 2015–2016. Our inversions use customized and validated high-fidelity meteorological output from Weather Research Forecasting and Stochastic Time-Inverted Lagrangian model for South Coast Air Basin and innovatively employ a model resolution matrix-based metric to disentangle the spatiotemporal information content of observations as manifested through estimated fluxes. We partially track and constrain fluxes from the Aliso Canyon natural gas leak and detect closure of the Puente Hills landfill, with no prior information. Our annually aggregated fluxes and their uncertainty excluding the Aliso Canyon leak period lie within the uncertainty bounds of the fluxes reported by the previous studies. Spatially, major sources of CH₄ emissions in the basin were correlated with CH₄-emitting infrastructure. Temporally, our findings show large seasonal variations in CH₄ fluxes with significantly higher fluxes in winter in comparison to summer months, which is consistent with natural gas demand and anticorrelated with air temperature. Overall, this is the first study that utilizes inversions to detect both enhancement (Aliso Canyon leak) and reduction (Puente Hills) in CH₄ fluxes due to the unintended events and policy decisions and thereby demonstrates the utility of inverse modeling for identifying variations in fluxes at fine spatiotemporal resolution.

1. Introduction

Methane (CH₄) is a powerful greenhouse gas that controls key aspects of atmospheric chemistry, air quality, and climate (Ciais et al., 2014). Regional and urban CH₄ budgets remain highly uncertain, and irreconcilable discrepancies exist between top-down and bottom-up estimates for even the largest components (Dlugokencky et al., 2009; Kirschke et al., 2013). To overcome these discrepancies, significant investments have been made in California to increase coverage and frequency of CH₄ measurements. Nowhere this is more apparent than in Southern California where wide array of sensors have been deployed in recent years to continuously monitor CH₄ emissions. This urgency is supported by the state of California that has adopted stringent targets for reducing CH₄ emissions to mitigate the impacts of climate change (e.g., SB1383; Bill Text SB-1383). The recently approved California law AB1496 states, “there is an urgent need to improve the monitoring and measurement of methane emissions from the major sources in California” and in particular “high-emission methane hot spots in the State.”

The Los Angeles megacity spanning a large fraction of the South Coast Air Basin (SoCAB) generates over 20% of the state’s CH₄ emissions (Jeong et al., 2016), and hence, mitigation is key to California meeting its reduction targets. However, effective mitigation is challenging given the spatially heterogeneous and sectorally diverse nature of CH₄ sources in this region (Hopkins et al., 2016). There is a large variety of CH₄-producing activities in the SoCAB, including oil and gas production fields, natural gas transmission, storage and distribution systems, petroleum refineries, landfills, wastewater treatment facilities, and

dairies (Carranza et al., 2018). Existing top-down studies at most provide spatially aggregated (basin total) monthly CH₄ emission estimates for the SoCAB (Wong et al., 2016). Gridded bottom-up annual inventories (~10 km) are too coarse to identify individual sources (Jeong et al., 2012; Maasackers et al., 2016), and downscaled versions of state-wide CH₄ emissions inventories have been found to consistently underestimate SoCAB emissions compared to top-down atmospheric studies (Cui et al., 2015; Jeong et al., 2016; Peischl et al., 2013; Santoni et al., 2014; Wecht et al., 2014; Wennberg et al., 2012; Wong et al., 2016; Wunch et al., 2009, 2016). On-road field surveys of near-surface CH₄ hot spots provide insight into spatial gradients for selected transects across the urban domain and verification of selected point sources (Hopkins et al., 2016). However, such surveys lack the persistence necessary to characterize the temporal variability of episodic emission sources that periodic airborne campaigns suggest are common in California (Duren et al., 2017).

To overcome these monitoring problems in the SoCAB, a network of 15 in situ sites have been progressively deployed since 2014. This network provides an unprecedented capability to determine spatiotemporal variability of CH₄ emissions at a fine spatiotemporal resolution. In this study, we utilize CH₄ measurements from this network and combine it with output from meteorological models tailored for the SoCAB to obtain inverse estimates of CH₄ emissions and their uncertainty at fine spatiotemporal resolution. This allows us to provide subbasin estimates of CH₄ emissions and spatio-temporally identify its anomalies in the basin. A methodological advancement in rapidly (near real time) identifying these anomalies through inverse modeling that does not rely on tailored meteorological output is presented in Ware et al. (2019).

2. Objectives and Analysis Steps

In this work, we combine in situ measurements of atmospheric CH₄ concentrations with inverse modeling to (1) characterize basin- and subbasin-scale temporal variability in fluxes including the onset and disappearance of large CH₄ sources, (2) identify the locations of the major sources of CH₄ emissions in the basin, and (3) evaluate the ability of a relatively sparse measurement network to update fluxes and identify spatiotemporal anomalies. As a test case for identifying anomalies, our analysis period spans the massive Aliso Canyon gas leak from late October 2015 through mid-February 2016 (Conley et al., 2016), that is, the second largest known and independently quantified natural gas release in the United States. Additionally, our analysis succeeds closure of the Puente Hills landfill whose impact on subbasin-scale inverse estimates of fluxes is compared with the previously reported fluxes for this facility.

3. Inversion Setup

3.1. Spatiotemporal Resolution of Inversions

CH₄ fluxes in this work are estimated for the SoCAB (Figure 1) at 0.03° spatial (1,826 grid cells) and 4-day temporal resolution from 28 January 2015 to 24 December 2016. We chose this spatiotemporal resolution to maintain an appropriate balance between degrees of freedom and number of fluxes that are estimated for a given temporal window. Thus, for most 4-day inversion windows we wanted to have an approximate ratio of 1:10 between observations and estimated fluxes, which was achieved for the spatiotemporal resolution mentioned above. For computational efficiency, inversions were performed for two 4-day periods at a time while maintaining an overlap of a 4-day period.

3.2. Observations and Background Estimate

The LA megacities in situ monitoring network currently consists of 15 urban sites; however, due to data availability and the sensitivity of sites to fluxes in the study area, only nine in the urban domain and one background site (Figure 1) were used in this study. Each site provides near-continuous measurements of boundary layer CH₄ concentrations (see Verhulst et al., 2017). Figure 2a illustrates the time series of 4-day average CH₄ enhancements at each site using background estimated from measurements obtained from San Clemente Island (Verhulst et al., 2017). This background was determined by applying the technique described in Thoning et al. (1989) that looks at the stability criteria (within hour and hour-to-hour variability) to estimate CH₄ background levels from several coastal and continental measurement sites in Southern California. We accounted for the uncertainty in the background estimate in inversions by imposing a lower limit of 0.04-ppm error in model-data mismatch (for definition, see section 3.3) before optimizing for

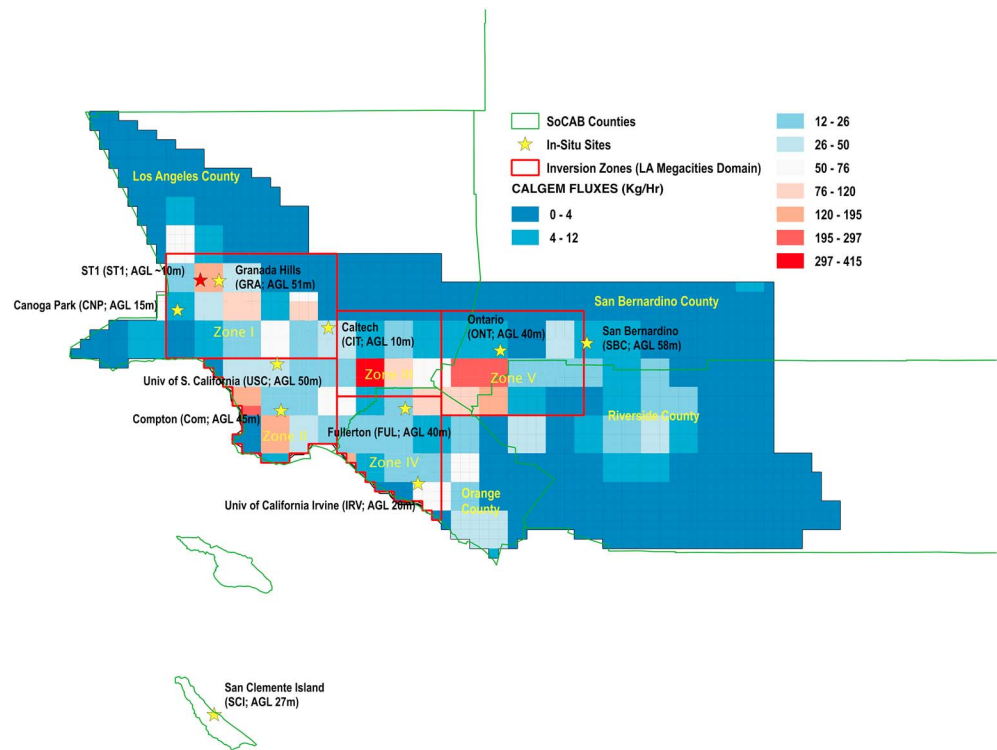


Figure 1. Study domain with name, three-letter code of the in situ measurement sites used in this study, and inlet heights above ground level. The San Clemente Island site is outside the flux inversion domain, and its measurements are used only to obtain background CH₄ concentrations. This map also depicts the best spatially resolved prior CH₄ emissions map for the South Coast Air Basin (SoCAB) from the California Greenhouse Gas Emissions Measurement (CALGEM; Jeong et al., 2012) version 2.2 inventory. As the resolution of CALGEM is 0.10°, an area weighted mass distribution of emissions at 0.03° is plotted in this figure and the same was used in inversions. The five subbasin inversion zones (Figure 3b) are described later and provided here for reference.

covariance parameters. This estimate encompasses the overall uncertainty in the enhancement due to the measurement technique and uncertainty in the background estimates from individual sites as well as coastal versus continental sites (see Figures 4b, 4d, and S10 in Verhulst et al., 2017). To ensure well-mixed conditions, we only used afternoon measurements from 12 to 4 p.m. when wind speeds were typically between 2 and 9 m/s. The temporal coverage of observations is illustrated in Figure 2b. (Note that for an extended period in 2016, observations from only six sites were available.) To avoid introducing a positive bias in the flux estimates, two negative enhancements that occur after subtracting the background were retained in inversions.

3.3. Inversion Methodology

We estimated CH₄ fluxes using a geostatistical inverse modeling (GIM) approach (e.g., Fang et al., 2014; Gourdjji et al., 2008; Michalak et al., 2004; Shiga et al., 2014), the objective function for which can be given as

$$L_{s,\beta} = \frac{1}{2} (\mathbf{z} - \mathbf{H}\mathbf{s})^T \mathbf{R}^{-1} (\mathbf{z} - \mathbf{H}\mathbf{s}) + \frac{1}{2} (\mathbf{s} - \mathbf{X}\boldsymbol{\beta})^T \mathbf{Q}^{-1} (\mathbf{s} - \mathbf{X}\boldsymbol{\beta}) \quad (1)$$

where $\mathbf{z}_{(n,1)}$ are hourly CH₄ measurements, $\mathbf{H}_{(n,p)}$ is a Jacobian matrix representing the sensitivity of measurements to underlying flux, $\mathbf{s}_{(p,1)}$ are the CH₄ fluxes, $\mathbf{R}_{(n,n)}$ is the model-data mismatch error covariance matrix, $\mathbf{X}_{(p,k)}$ is a matrix of covariates, $\boldsymbol{\beta}_{(k,1)}$ are the coefficients or weights of individual covariates, and $\mathbf{Q}_{(p,p)}$ is the error covariance matrix (also known as prior covariance) that describes the deviations of \mathbf{s} from $\mathbf{X}\boldsymbol{\beta}$.

As in earlier studies, \mathbf{s} and $\boldsymbol{\beta}$ are estimated as part of the inversion, yielding optimal values, that is, $\hat{\mathbf{s}}$ and $\hat{\boldsymbol{\beta}}$. \mathbf{H} is obtained from the Weather Research Forecasting (WRF)-Stochastic Time-Inverted Lagrangian Transport

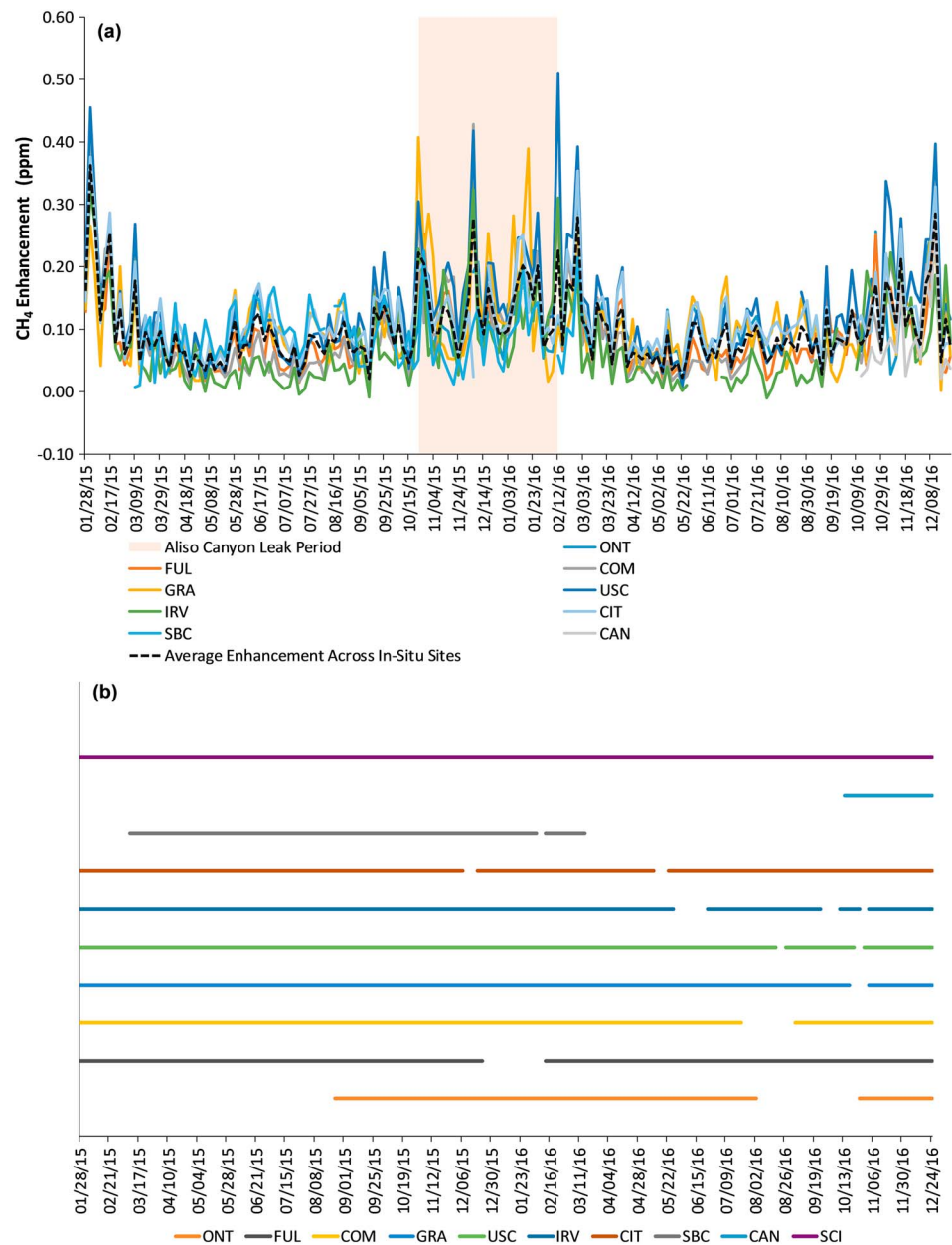


Figure 2. (a) Average 4-day CH₄ enhancements for the nine in situ sites. (b) The time period of observation availability for the nine in situ sites. In (a) the black dashed line shows mean CH₄ enhancements across all sites at 4-day interval for which observations were available. The period of unavailability of observations is reported as gaps in the horizontal line for a site in (b).

(STILT) model (see section 4 for details), and parameters for **R** and **Q** are computed through restricted maximum likelihood (see Gourdji et al., 2010; Michalak et al., 2004). In this work, California Greenhouse Gas Emissions Measurement (CALGEM) version 2.1 (e.g., Figure 1), an inventory of CH₄ emissions (Jeong et al., 2012), was prescribed as a covariate in **X**. A separate variance was computed for each tower in **R**, and a scaling factor was computed for **Q** whose off-diagonal entries were 0 and diagonal entries contained CALGEM emission estimates for each grid cell (e.g., Yadav et al., 2016).

We used Lagrange multipliers to impose a nonnegativity constraint on inverse estimates of CH₄ fluxes to avoid nonphysical negative fluxes (see Miller et al., 2014). Imposing nonnegativity constraints makes

analytical uncertainty computation untenable; therefore, we adopted a simulation-based approach to derive flux uncertainties.

Given a predetermined \mathbf{z} , \mathbf{H} , and \mathbf{X} , only parameters of \mathbf{R} and \mathbf{Q} regulate the estimate of $\hat{\mathbf{s}}$ and $\hat{\boldsymbol{\beta}}$ in GIM. Therefore, to estimate grid-scale uncertainty on $\hat{\mathbf{s}}$, first we use restricted maximum likelihood to obtain \mathbf{R} and \mathbf{Q} parameters and their posterior error covariance from the inverse of the observed Fisher information matrix (e.g., Kitanidis, 1995, 1996). In the next step, we generate 1,000 samples of \mathbf{R} and \mathbf{Q} parameters from this posterior error covariance through the Cholesky decomposition (see Michalak et al., 2004 for details on the procedure for generating these realizations) and use them to compute 1,000 realizations of $\hat{\mathbf{s}}$ from the standard GIM equations given in Michalak et al. (2004). Further, we impose non-negativity on these 1,000 realizations of $\hat{\mathbf{s}}$ using Lagrange multipliers, and the standard deviation of these 1,000 realizations is considered as posterior uncertainty on grid-scale fluxes. The sum of the grid-scale posterior uncertainty is the basin-wide uncertainty as shown in Figure 5a. Overall, this process of estimating uncertainty results in more conservative estimates in comparison to other methods including Markov chain Monte Carlo (see Jeong et al., 2012) and analytical and conditional simulations (see equations in Michalak et al., 2004). Computationally, for a 4-day period, it took 4 to 8 hr to compute these 1,000 realizations, but as most of these runs were completed on a supercomputer, the uncertainty estimate for all 175 four-day periods were obtained within a day.

3.4. Evaluation Metrics for Inversions

We used the following: (1) correlation and root mean square error (RMSE) between observations (\mathbf{z}) and convolution of estimated fluxes with transport ($\mathbf{H}\hat{\mathbf{s}}$), (2) time series of the trace or the diagonal of the model resolution matrix scaled (e.g., divided) by the count of observations (n), and (3) reduced chi-square statistic to evaluate the performance of our inversions. Out of these three metrics, the first one is routinely employed to evaluate performance of inverse models.

The second metric, that is, the model resolution matrix or an averaging kernel matrix (for details see, Aster et al., 2018; Tarantola, 2004) describes the closeness between the unknown true fluxes and the inverse estimates of fluxes. The model resolution matrix is of considerable utility as it (1) has a definite lower and upper bound (range of 0–1), (2) encompasses information about the posterior uncertainty on the estimated fluxes, (3) conveys information regarding the spatiotemporal sensitivity of the network, and (4) leads to identification of the grid-scale fluxes that are constrained by the measurements. This matrix for GIM (e.g., Yadav et al., 2016) can be given as

$$\hat{\mathbf{m}} = \boldsymbol{\Lambda}\mathbf{H} \quad (2)$$

where \mathbf{H} is as defined earlier and $\boldsymbol{\Lambda}_{(p,p)}$ can be written as

$$\boldsymbol{\Lambda} = \mathbf{X}(\mathbf{X}^T\mathbf{H}^T\boldsymbol{\psi}^{-1}\mathbf{H}\mathbf{X})^{-1}\mathbf{X}^T\mathbf{H}^T\boldsymbol{\psi}^{-1} + \mathbf{Q}\mathbf{H}^T\boldsymbol{\psi}^{-1} - \mathbf{Q}\mathbf{H}^T\boldsymbol{\psi}^{-1}\mathbf{H}\mathbf{X}(\mathbf{X}^T\mathbf{H}^T\boldsymbol{\psi}^{-1}\mathbf{H}\mathbf{X})^{-1}\mathbf{X}^T\mathbf{H}^T\boldsymbol{\psi}^{-1} \quad (3)$$

and

$$\boldsymbol{\psi} = \mathbf{H}\mathbf{Q}\mathbf{H}^T + \mathbf{R} \quad (4)$$

As an outcome of inversion, if $\hat{\mathbf{m}}_{(p,p)}$ is an identity matrix, then we would perfectly estimate the true fluxes. In this ideal case of perfect resolution of fluxes, $\text{Tr}(\hat{\mathbf{m}})$ (note the symbol Tr denotes the trace of a matrix) would be equal to the number of estimated fluxes and the uncertainty on the estimated fluxes would be 0. However, as atmospheric inverse problems are mostly underdetermined, $\text{Tr}(\hat{\mathbf{m}})$ is less than or equal to the number of measurements. Even in the ideal case of $\text{Tr}(\hat{\mathbf{m}}) = n$, it is unlikely that the flux of a particular grid cell is perfectly resolved; that is, it has a value of 1 along the diagonal of $\hat{\mathbf{m}}$. This happens due to the presence of uncertainty associated with observations, transport, and prior, which prevents perfect resolution of the true grid-scale fluxes, that is, grid cells with identity diagonal entries. In such situations, the resolution is spread over multiple grid cells indicated by the off-diagonal entries in $\hat{\mathbf{m}}$ with the diagonal entries closer to 1 having less spread in comparison to the diagonal entries closer to 0. Regardless, as uniquely employed in this study,

Table 1
WRF Configuration Parameters

Option	Description
Land surface	Noah land-surface model with Monin-Obukov (Janic) surface layer
Urban canopy	None
PBL package	MYNN 2.5-level scheme
LW radiation	RRTMG
SW radiation	RRTMG
Microphysics	WSM five-class scheme
Convection	Grell 3D (only in domains d01 and d02)
Nesting	One way
Nudging	None
Advection	Fifth-order horizontal, third-order vertical monotonic advection for moisture and scalars
Diffusion	Second-order horizontal diffusion using Smagorinsky first-order closure

Note. WRF = Weather Research Forecasting; PBL = planetary boundary layer; LW = longwave; SW = shortwave; MYNN = Mellor-Yamada-Nakanishi-Niino; RRTMG = Rapid Radiative Transfer Model Global; WSM = WRF-Single-Moment.

a threshold based on the diagonal entries of $\hat{\mathbf{m}}$ can still be defined to identify regions of large emissions, for areas well constrained by the network.

The third metric for evaluating inversions can be obtained by computing χ^2 statistic and dividing it by degrees of freedom ν , which is equal to, $\text{rank}(\mathbf{H})$ or n . This reduced chi-square statistic (χ_{red}^2) can be given as

$$\chi^2 = (\mathbf{z} - \mathbf{H}\hat{\mathbf{s}})^T \mathbf{R}^{-1} (\mathbf{z} - \mathbf{H}\hat{\mathbf{s}}) + (\mathbf{s} - \mathbf{X}\hat{\boldsymbol{\beta}})^T \mathbf{Q}^{-1} (\mathbf{s} - \mathbf{X}\hat{\boldsymbol{\beta}}) \quad (5)$$

$$\chi_{\text{red}}^2 = \frac{(\mathbf{z} - \mathbf{H}\hat{\mathbf{s}})^T \mathbf{R}^{-1} (\mathbf{z} - \mathbf{H}\hat{\mathbf{s}}) + (\mathbf{s} - \mathbf{X}\hat{\boldsymbol{\beta}})^T \mathbf{Q}^{-1} (\mathbf{s} - \mathbf{X}\hat{\boldsymbol{\beta}})}{\nu} \quad (6)$$

where all symbols are as described above.

No effort was made to forcibly scale variances in \mathbf{R} and \mathbf{Q} to achieve a χ_{red}^2 of 1, as we completely relied on restricted maximum likelihood to provide these estimates. The χ_{red}^2 statistic should always be seen in conjunction with $\text{Tr}(\hat{\mathbf{m}})$. In an unconstrained inversion, as χ^2 reduces, variance in \mathbf{R} increases, which leads to an increase in $\text{Tr}(\hat{\mathbf{m}})$. This quantity can never be higher than ν or the number of observations used in the inversion. Additionally, χ_{red}^2 itself is subject to uncertainty (σ) due to random noise in the data, and this σ is equal to $\sqrt{2/n}$, and therefore, any model with $\chi_{\text{red}}^2 \pm \sqrt{2/n}$ can be considered as a true model (e.g., Andrae et al., 2010).

In this study, due to the imposition of nonnegativity, the objective function in equation (1) does not remain linear, and therefore, degrees of freedom are strictly not defined and $\hat{\mathbf{m}}$ cannot be computed. Even under these conditions, $\hat{\mathbf{m}}$ and χ_{red}^2 computed from an unconstrained inversion whose solution of $\hat{\mathbf{s}}$ is normally close to the nonnegative $\hat{\mathbf{s}}$ provide useful information for analysis and understanding the quality of the model fit. Thus, $\hat{\mathbf{m}}$ computed from the unconstrained inversion is used in this study for hot spot detection (i.e., area of large CH_4 emissions; see section 5.2), and χ_{red}^2 obtained after imposition of nonnegativity is used to assess the quality of model fit.

4. Atmospheric Transport and SoCAB CH_4 Enhancements

4.1. Modeling Framework for Obtaining Jacobian or Sensitivity Matrices for Inverse Modeling

In this work, the sensitivity of the CH_4 observations to surface fluxes was obtained by using a version of WRF model optimized for the SoCAB (Feng et al., 2016) and coupled to the STILT model (STILT; Lin et al., 2003).

Previously, the WRF-STILT framework has been utilized in many studies for estimating fluxes (e.g., Chang et al., 2014; Henderson et al., 2015). Our WRF-STILT model used mass-coupled, time-averaged WRF fields from a triply nested setup with 51 vertical levels and horizontal grid spacing of 12, 4, and 1.33 km (same as in Feng et al., 2016). We used WRF version 3.6.1 with the physics and other model configuration selections summarized in Table 1. We used the settings corresponding to configuration MYNN_d03 in Feng et al. (2016). In comparison to Feng et al., we decided not to use the urban canopy model in our WRF runs, as we did not see an improvement in terms of better score with respect to evaluation metrics for inversions from including an urban canopy model (e.g., Nehrkorn et al., 2018).

WRF meteorological fields were verified for the entire duration of this study starting from 28 January 2015 to 24 December 2016 against hourly observations available from surface profilers, and upper air data collected as part of Aircraft Communications, Addressing, and Reporting System (ACARS) from 42 surface observation sites within the SoCAB. Mean wind speeds agreed with ACARS profiler observations and were within 0.5 m/s with RMSEs generally below 2.5 m/s. Similarly, thermal profiles were also in good agreement, with mean potential temperature errors below 0.5 K and RMSE mostly lower than <2.5 K. Surface station error statistics showed some variability by location and season but did not reveal systematic domain-wide biases in either temperature or wind speed.

We did not perform any planetary boundary layer height (PBLH) comparison against ceilometer (Morris, 2016) data, since these were not available. We did look into using ACARS profiler data for PBLH verification

but found that the estimates of PBLH from these data were not reliable to allow a meaningful comparison against WRF. Due to this reason, we restricted our use of ACARS profiler data to point-by-point comparison of winds and temperature. This comparison with winds and temperature is shown in the supporting information of the manuscript (coauthored by the author) that uses the same WRF-STILT output as in this study and has been accepted for publication in the *Journal of Geophysical Research: Atmospheres* (see Ware et al., 2019).

4.2. Assessment of Sensitivity at In Situ Towers

Modeled atmospheric transport plays a critical role in inverse estimation of CH₄ fluxes. The relationship between \mathbf{H} and the observed CH₄ enhancement at individual towers reveals how well the atmospheric transport model captures the sensitivity (\mathbf{H}) of the observations to surface fluxes. Strong correlation or coherence between sensitivity and enhancement indicates better representation of the atmospheric transport and is a necessary condition for obtaining robust flux estimates.

To study this correlation for an in situ site, we first summed up CH₄ observations (enhancements) within a 4-day period and then divided it by total observations to obtain an average enhancement. Similarly, we summed up sensitivity or \mathbf{H} across space (1,826 grid cells) to come up with a single value for sensitivity for an in situ site for a 4-day period. For a basin-wide assessment these averages were computed by combining observations and sensitivity from all available sites for a given 4-day period.

Overall, we observed a strong correlation between CH₄ enhancements and the combined sensitivity of our tower network (e.g., Figures 3a and 3b); however, large variations in this relationship were observed at different sites (e.g., Figure 4). Outliers (high sensitivity and low enhancement or high enhancement and low sensitivity) at all towers reduced the strength of the enhancement-sensitivity correlation. In fact, we observed considerably more outliers at the Granada Hills (GRA) tower than at other sites. This result was consistent with the challenges in modeling meteorology at GRA, which is located near the base of a mountain pass and in a region of complex terrain. We account for the magnitude of the correlation between sensitivity and enhancement in \mathbf{R} where the application of restricted maximum likelihood results in larger uncertainty for in situ sites that exhibit poor correlation between sensitivity and CH₄ enhancement. Note that other than the minimum bound of 0.04 ppm due to the background, we do not further artificially inflate errors in \mathbf{R} . The increase in error in \mathbf{R} on top of the background includes error due to transport, measurement, and aggregation (e.g., Engelen et al., 2002), that is, solely the result of the optimization through restricted maximum likelihood.

In the following sections, we explore the impact of the network and transport on flux estimation, including the sensitivity for 4-day inversion windows as well as the overall spatial and temporal completeness of the inversion.

5. Results and Discussion

In the following sections we (1) report variability of the aggregate fluxes for the SoCAB; (2) spatially resolve fluxes within the SoCAB; (3) provide estimates of net CH₄ fluxes for five zones, which lie within the area of study; and (4) assess the impact of directional network sensitivity on inversion performance.

5.1. Temporal Variability in SoCAB Total CH₄ Fluxes

Figure 5a illustrates the time series of posterior CH₄ fluxes and their uncertainties for the SoCAB over the 2-year period of this study including the Aliso Canyon leak period (October 2015 through mid-February 2016).

We first evaluate the nonleak periods in 2015 and 2016. Strong seasonality was observed in both the SoCAB fluxes and the basin mean CH₄ enhancements (e.g., Figures 5a and 5b), which led to a difference of ~ 20 Mg/hr in the mean basin flux between summer (June and July 2016) and winter months (November and December 2016). This agrees with the prior work using independent top-down (tracer-tracer) flux estimation methods by Wong et al. (2016), which showed significant variability in monthly top-down CH₄ emissions estimates. In this study (Wong et al., 2016), a larger peak in winter that cannot be attributed to landfill emissions (see section 4.5 in Wong et al., 2016, and K. Spokas et al., 2015; K. A. Spokas & Bogner, 2011) and smaller peak in the late summer/early fall in CH₄ emissions was observed.

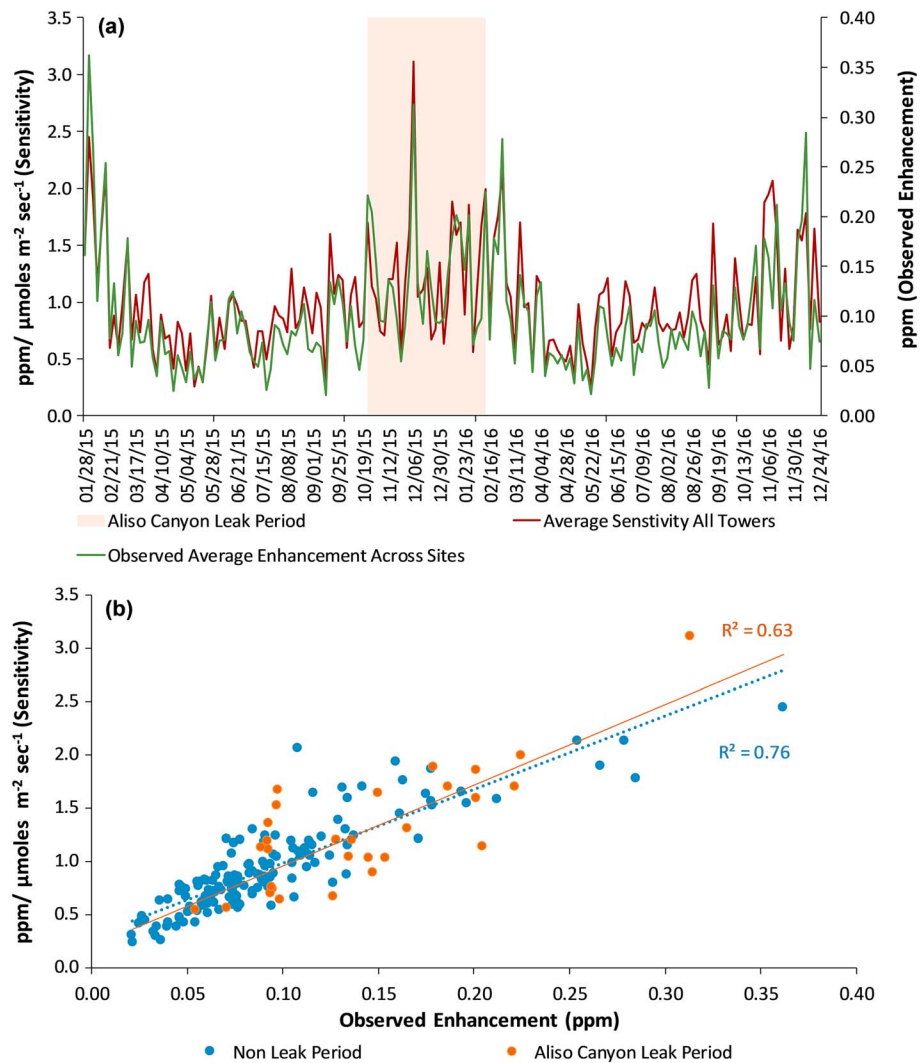


Figure 3. (a) Time series of 4-day average sensitivity and observed enhancements at eight in situ towers used in inversions. (b) Relationship between the two time series shown in (a). To obtain average basin-scale sensitivity, we first summed the grid-scale sensitivity of observations of an in situ site within a 4-day period and then divided it by the count of observations for that site.

As in Wong et al. (2016) our observed seasonality of CH_4 fluxes was anticorrelated with average air temperature with $r = 0.56$ (e.g., Figure 5a) and potentially implies moderate dependence of CH_4 fluxes on heating demand in winter months and natural gas infrastructure (Wunch et al., 2016). Overall, this correlation is also visible in the monthly natural gas deliveries to residential customers in California and CH_4 enhancements (e.g., <https://www.eia.gov/naturalgas/monthly/>). However, the strength of association of enhancements with air temperature or heating demand varies at each in situ site. This is clearly visible in Figure 2a, which shows variations in the magnitude of the seasonality in enhancements at each in situ site and is an outcome of the differences in the meteorological conditions because of complex terrain, spatial distribution of population, and spatial distribution and composition of the CH_4 -emitting infrastructure.

After excluding the Aliso Canyon gas leak period, we estimated the mean annual SoCAB CH_4 flux for 2015–2016 to be $\sim 38 \pm 10$ Mg/hr. Our estimate was within the range of values reported in previous studies (see Figure 6). Indirectly, we validated our annual mean estimate by forward transporting the CALGEM emissions. This process can be expressed through equations (7) and (8) whereby in the first step we forward transport CALGEM through \mathbf{H} and then in the second step we compute the ratio R_o of the modeled (MD) and

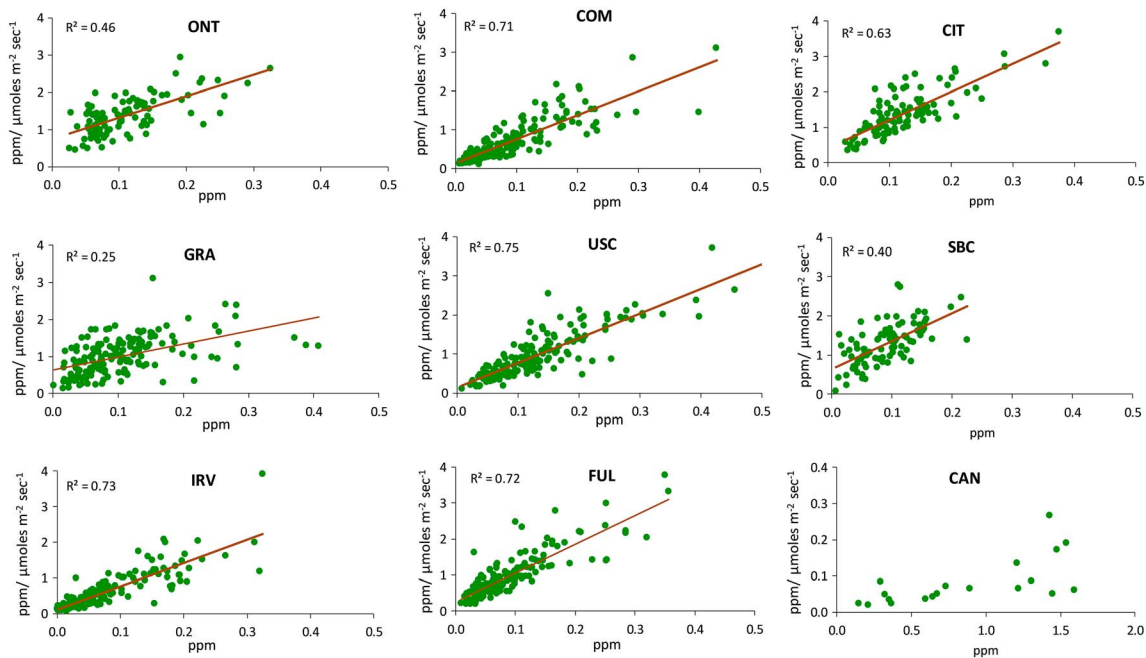


Figure 4. Relationship between average 4-day enhancement and sensitivity for nine in situ sites used in this study. This relationship is shown on the same scale for all sites except Canoga Park (CAN). Observations from CAN were only available from 20 October 2016 and, comparatively, over the short duration of approximately 2 months a considerably reduced sensitivity to large enhancements was observed at this site. This creates problems in plotting CAN on the same scale as all other sites. Additionally, due to data deficiency, no trend was computed for this site.

observed enhancements (OE), which after excluding the Aliso Canyon period was 96% in this study (Figure 7) that is, a flux of ~ 37.8 Mg/hr.

$$MD_{(n,1)} = H_{(n,p)} \times CALGEM_{(p,1)} \quad (7)$$

$$R_o = \left(\frac{\sum_{i=1}^n \frac{MD_i}{OE_i} \times 100}{n} \right) \quad (8)$$

However, this is the mean estimate and hides the fact that the temporally static CALGEM inventory likely results in significant underestimation and overestimation of the observed CH_4 enhancements during winter and summer months, respectively.

5.2. Spatial Distribution of CH_4 Fluxes Across the SoCAB

Using inverse modeling to spatially resolve CH_4 emissions was challenging as it involved identifying the impact of measurements in updating the estimated grid-scale fluxes. In this study, the signal of enhanced fluxes at the beginning of the Aliso Canyon leak was evident in both enhancements and the estimated basin-scale fluxes. This allowed us to determine the pulse of the model resolution, that is, the value along the diagonal of the model resolution for the grid cell containing Aliso Canyon that lead to its impact being felt on the basin-scale fluxes (see Figure 8). In this work, we used a conservative model resolution threshold of 0.06 to filter grid-scale fluxes from the nonleak period. This was the highest model resolution during the Aliso Canyon leak period that also coincided with the largest fluxes at the beginning of the leak period (see section 5.3). Note that we do not claim that the diagonal of the model resolution should be at least 0.06 to adjust the prior flux as this depends on the network coverage, sensitivity to emissions, and the information content of measurements. For the present in situ measurement network, we found this limit should be no less than 0.01, the boundary of which is shown in Figure 9. We define the Los Angeles megacity domain as the area bounded by the contour of 0.01 that as reported by CALGEM represents 80% of the total SoCAB flux. The inversion has reduced sensitivity for a larger subset of the SoCAB, that is, the area bounded by the contour of 0.001 that is representative of 94% of the CALGEM total for that domain.

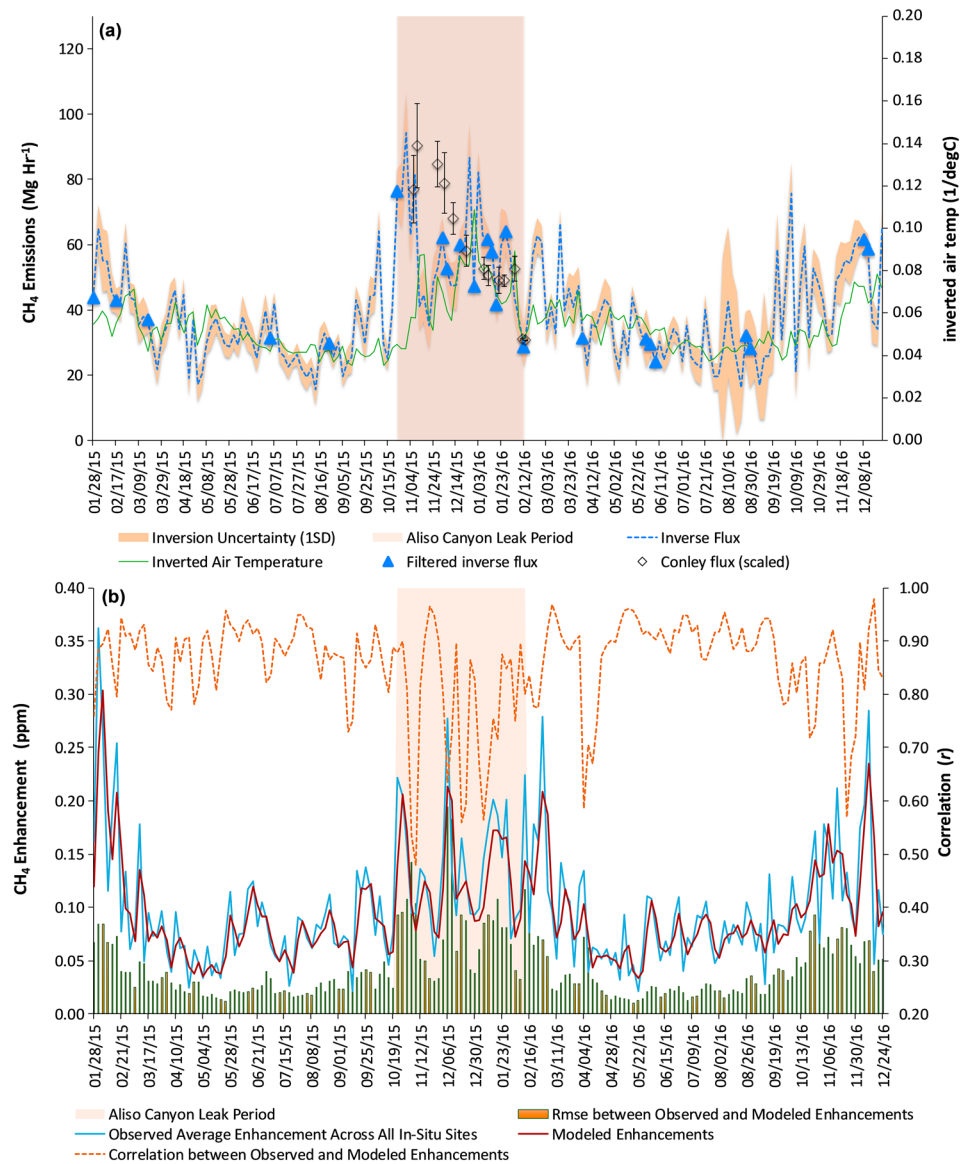


Figure 5. (a) Posterior CH₄ fluxes and uncertainties (shaded orange area above and below the dotted blue curve of the estimated inverse flux) for the South Coast Air Basin domain from 28 January 2015 to 24 December 2016. The period of the Aliso Canyon blowout is highlighted, with black diamonds indicating facility-scale leak rate reported by Conley et al. (2016). Those leak estimates are converted to an approximate basin-scale total fluxes by adding the observed preleak mean CH₄ flux of ~ 30 Mg/hr that is assumed constant for this comparison (section 6.3). Inverse air temperature is computed by aggregating 4-day average daily temperature recorded at eight major airports across the study domain. Blue triangles indicate filtered posterior fluxes based on the methodology described in section 5.5.1. (b) Metrics of inversion performance. The time series of measured and modeled mean enhancements at 4-day interval are plotted on the primary axis, and the root mean square error (RMSE) and correlation between those curves within a 4-day period is plotted on the primary and secondary axes, respectively.

To detect and locate large CH₄ flux anomalies in the SoCAB, we computed mean grid-scale fluxes for the entire nonleak period by identifying grid cells whose model resolution was ≥ 0.06 for at least ten 4-day time periods, which covered 24% of the SoCAB and 67% of the fluxes reported in CALGEM. This does not bound the upper limit on the sample size of the 4-day time periods, which leads to an unequal number of 4-day flux estimates that are used to compute mean grid-scale flux, thereby biasing these estimates. However, the goal of this exercise was not to accurately compute mean flux but to identify major sources of CH₄ emissions, which in Figure 10a are bounded by the contours of 100 kg/hr. Many of the sources in Figure 10a are

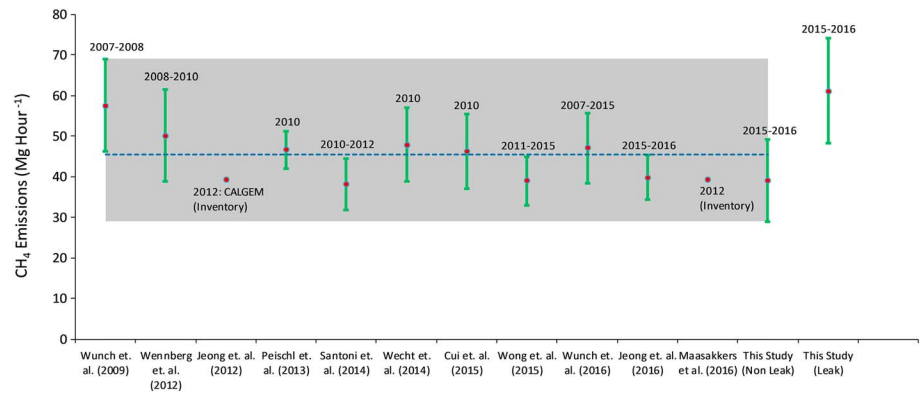


Figure 6. Annual estimates of CH₄ emissions for the South Coast Air Basin (SoCAB) reported by previous studies. The studies are listed by the year of publication, and the data used for these publications are mentioned at the top of emission estimates. Most of these studies are based on the data collected as part of flight campaigns and are not truly representative of the mean annual flux for SoCAB (for details, see individual publications). Couple of studies, that is, Wong et al. (2016) and Wunch et al. (2016), utilize Fourier transform spectrometer to measure column XCH₄ to compute fluxes. The range of the flux estimates inclusive of uncertainty (max and min) of previous studies is highlighted, and the mean across these studies is plotted as a dotted line.

associated with the facilities listed in the high-resolution Vista-LA database of likely CH₄-emitting facilities (Carranza et al., 2018) and are not present in CALGEM. The total flux for the area bounded by the contour of 0.06 model resolution is approximately similar in the CALGEM (bottom-up) and inversions (top-down). However, the spatial distribution of the fluxes is remarkably different (compare Figures 1 and 10a).

5.3. Detecting Major Flux Anomalies

The Aliso Canyon gas leak and its sustained perturbation of the SoCAB CH₄ fluxes offered an unprecedented opportunity to test the ability of the inversion system to spatio-temporally resolve a large CH₄ flux anomaly.

The start and stop times and leak rates from this event were well constrained by independent reports (California Air Resources Board [CARB], 2016). The sudden onset of the leak was captured by our observation-inversion system at the basin scale (Figure 5a) with no prior information, since the inversion prior is static and did not include contribution from the Aliso Canyon. Although the grid cell containing Aliso Canyon had nonzero prior emissions, directly estimating fluxes at grid scale with our relatively sparse set of observations spread across the SoCAB translated to very large uncertainties. Therefore, to compare the inversion basin total flux with the localized facility leak rate, a mean SoCAB flux of 34 Mg/hr for the 2 months preceding the reported Aliso Canyon leak start on 23 October 2015 was used as a baseline flux. This resulted in an inversion-derived leak rate of 42 ± 10 Mg/hr between 23 and 27 October 2015 compared to the 47 ± 10 Mg/hr reported for the aircraft flight conducted on 7 November 2015 (Conley et al., 2016). It was not possible to produce a robust estimate of the total gas lost from the Aliso Canyon leak using the inversion given the significant periods of reduced sensitivity for the inversion and because of the strong seasonal variability in the rest of the basin flux. The Aliso Canyon leak period was also spatially detected by the inversion (e.g., Figure 11), although rapid mixing and overlapping footprint resulted in elevated fluxes for multiple sub-regions (Figure 10b), highlighting the difficulty of the current framework to properly allocate point source fluxes.

As another example, the CALGEM grid cell containing the Puente Hills landfill was previously reported to be the largest source of CH₄ emissions in the SoCAB. However, no such source appears in our

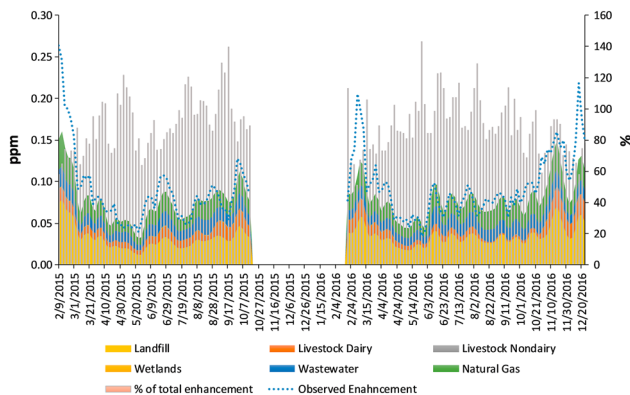


Figure 7. Aggregated sectoral California Greenhouse Gas Emissions Measurement (CALGEM) CH₄ emissions in accounting for observed average CH₄ enhancement (dashed blue line on the primary axis) across all in situ sites (see section 4.2 on the method used to compute observed average enhancement). The percentage of observed enhancement accounted by forward transporting sum of all sources of CALGEM emissions is shown as bars and plotted on the secondary axis for each time period (see equation (8) in section 5.1). Note that CH₄ emissions in CALGEM have no temporal variability, and therefore, observed variability in modeled sectoral concentrations is only due to atmospheric transport. Additionally, even though we show sectoral breakdown of CH₄ concentrations based on CALGEM inventory by forward transporting emissions from each sector in CALGEM, only total CH₄ emissions as expressed in equation (7) were used to compute the percentage of observed enhancement on the secondary axis.

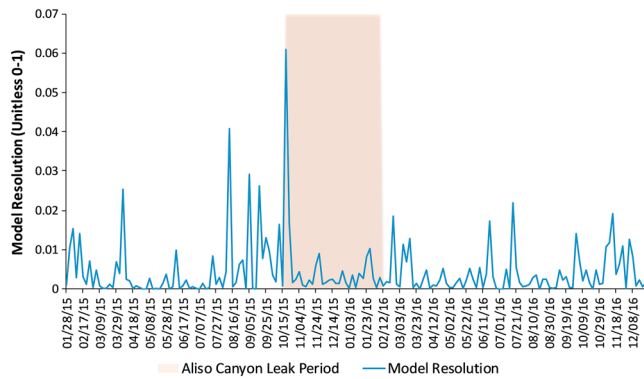


Figure 8. Time series of the diagonal entry of the model resolution matrix for the grid cell containing Aliso Canyon from 28 January 2015 to 24 December 2016.

inversion posterior estimate, and in fact, it is the lowest flux area in the basin. This reduction in a major emission source provides a converse example to the Aliso Canyon incident and may be due to the closure of the landfill in late 2013, well after the 2010 time period covered by the CALGEM.

5.4. Quantifying Fluxes and Variability for Key Zones of the Los Angeles Megacity

We evaluated subbasin-scale fluxes in five key zones of the Los Angeles megacity (Figures 1 and 10). These five zones were defined based on the coverage of the network and county boundaries and by imposing a requirement that at least 100 grid cells should be available within a subregion to compute fluxes. For each of these zones we computed mean CH₄ flux for the leak and nonleak periods. These mean fluxes were computed by using the flux data during the Aliso Canyon gas leak and data before and after the Aliso Canyon gas leak, respectively. This separation of flux

in two time periods allowed us to compute fluxes for anomalous (Aliso Canyon) and nonanomalous periods where the latter is representative of a flux period that provides an approximately accurate estimate of the mean CH₄ flux in the basin. Even though fluxes for 50 days spread over December, January, and February for a normal year (i.e., when the Aliso Canyon anomaly is absent) were not available, we think a mean flux computed from the remaining nonanomalous time periods is an adequate representation of the basin and zonal flux.

Overall, the mean CH₄ flux of Zone I, which includes Aliso Canyon, exhibited a large (~70%) statistically significant difference between the leak and nonleak periods (Figure 10b). These differences in the means were obtained without modifying the inversions, that is, arbitrarily creating a prior with higher flux or increasing prior uncertainty during the Aliso Canyon leak period. This result gives us confidence that urban-scale inverse modeling has the potential to detect anomalous flux events given a sufficiently large flux and sufficiently sensitive measurement network. Furthermore, we used a nonparametric Mann-Whitney *U* test (e.g., Mann & Whitney, 1947) that has no distributional assumptions and allows for unequal variance between samples for checking the incompatibility in CH₄ fluxes between 23 October and 26 December 2015 with 21 October and 24 December 2016, that is, a corresponding time duration in 2016 when the Aliso Canyon leak was absent. Within the context of the current study, assumption of unequal

variance allows for accommodation of differences in fluxes due to (1) variations in the sensitivity (**H**) of the observational network and (2) disparities in the processes governing CH₄ fluxes. To apply the Mann-Whitney *U* test, we compared spatially aggregated time series of CH₄ fluxes within nine grid cells that contained Aliso Canyon in Zone I. The test returned a *p* value <0.05 indicating that the two time series came from two different distributions. This result was also found to be applicable at the basin scale and for Zones I and II and happened even when the time period between October and December 2015 contained periods when the observation network was not sensitive to the Aliso Canyon leak, indicating that higher flux during the Aliso Canyon leak is not simply the result of larger seasonal flux in the SoCAB in winter months.

For Zone III, inversions resulted in CH₄ flux of $2,481 \pm 1,147$ kg/hr, which was considerably lower than 6,785 kg/hr reported by CALGEM. As described in the previous section, we attribute this reduction to the closure of the Puente Hills landfill in late 2013 (Department of Public Works, 2018; Los Angeles County, 2016). This was independently confirmed by the reduced CH₄ flux of 361 ± 55 kg/hr for Puente Hills reported by CARB from an aircraft flight for November 2017 (CARB, 2018), which was ~10 times lower than the flux of $3,881 \pm 1,130$ kg/hr reported by Peischl et al. (2013) for Puente Hills for May 2010. Combining flux

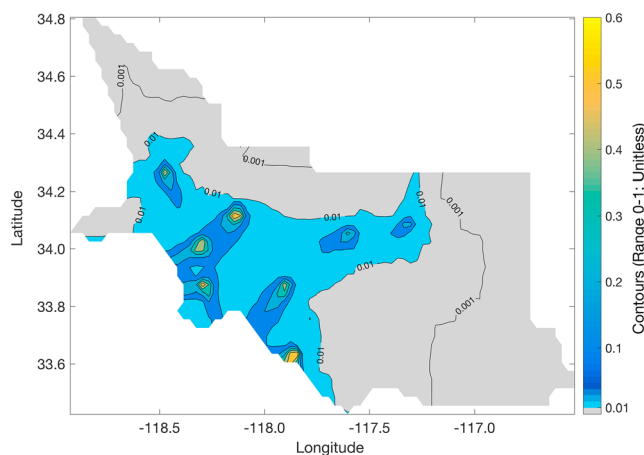


Figure 9. Contour plot of the 4-day average model resolution matrix over the full duration of the flux inversions. Contours of higher values indicate improved prior update or resolvability of the fluxes with a value of 1 being the maximum. The highest sensitivity to fluxes occurs near the in situ measurement sites used in the inversion.

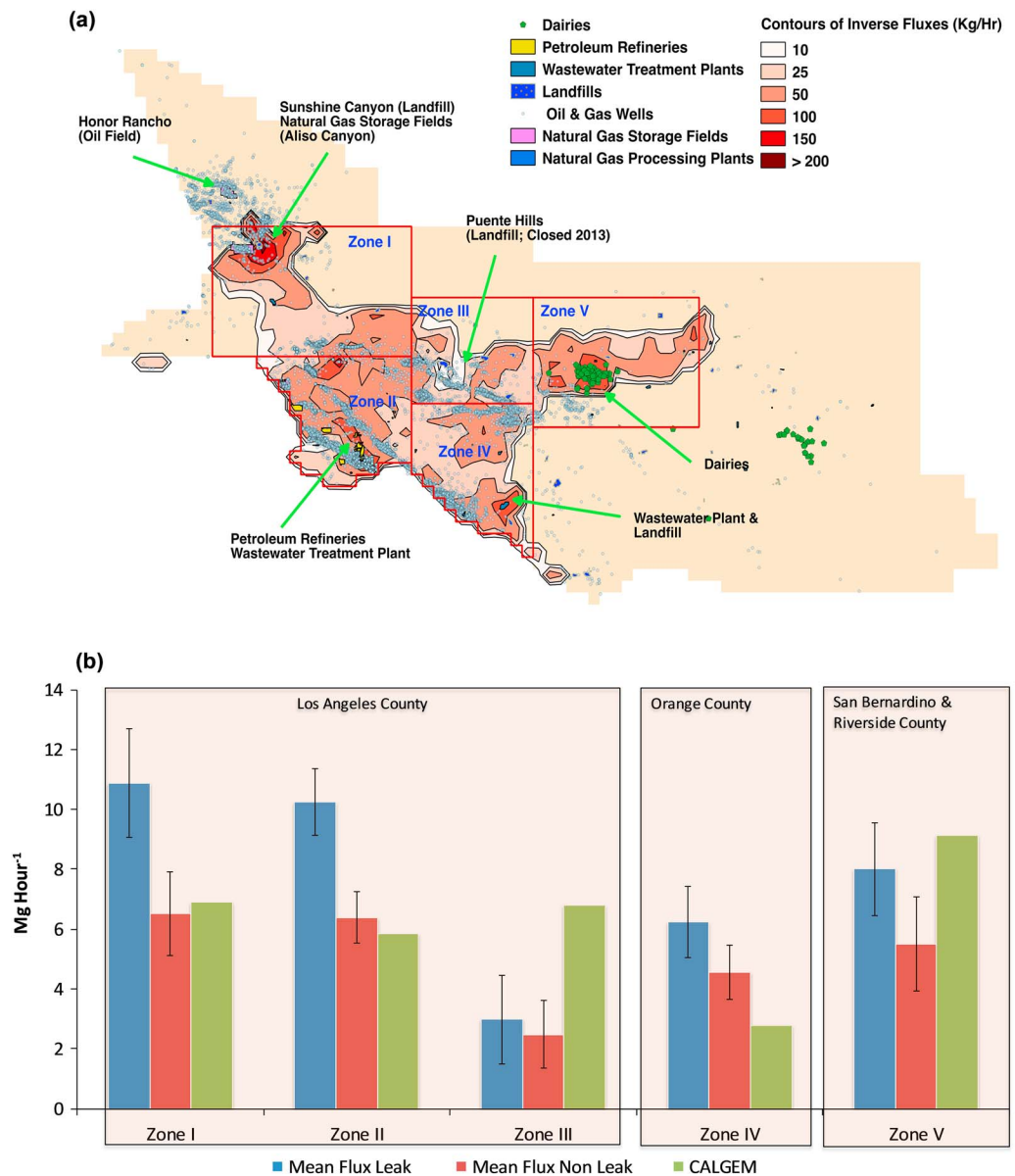


Figure 10. (a) Mean posterior CH₄ fluxes for the study period 2015–2016 excluding the 4-month Aliso Canyon leak period. The overlays indicate the locations of likely CH₄-emitting infrastructure (after Carranza et al., 2018; see details in section 5.2). The five red zones indicate focus areas within the Los Angeles megacity with key sources highlighted including the apparent disappearance of the Puente Hills landfill source following its closure in 2013. (b) Comparison of the inversion posterior fluxes (for both the Aliso Canyon leak period and the nonleak period) with 1-sigma uncertainties versus California Greenhouse Gas Emissions Measurement (CALGEM) for each of the five zones in (a). The impact on the basin-wide flux from the Aliso Canyon gas leak is readily apparent. We attribute the large reduction in the posterior fluxes in Zone III to the shutdown of the Puente Hills landfill in 2013.

estimate from Peischl et al. (2013) with our estimate of $2,481 \pm 1,147$ kg/hr for Zone III leads to a total flux that was similar to that reported by CALGEM inventory for this zone.

In addition to computing aggregated fluxes for these five zones, we also evaluated variability in fluxes for the five zones (Figure 11) over the study period. Zones I and II exhibited similar seasonal variability as the net basin flux (e.g., winter maxima), whereas the fluxes in the other zones were approximately constant. This suggests that a subset of sectors in the SoCAB (e.g., industrial and/or residential activity in Zones I and II) were responsible for the majority of the observed seasonal variability.

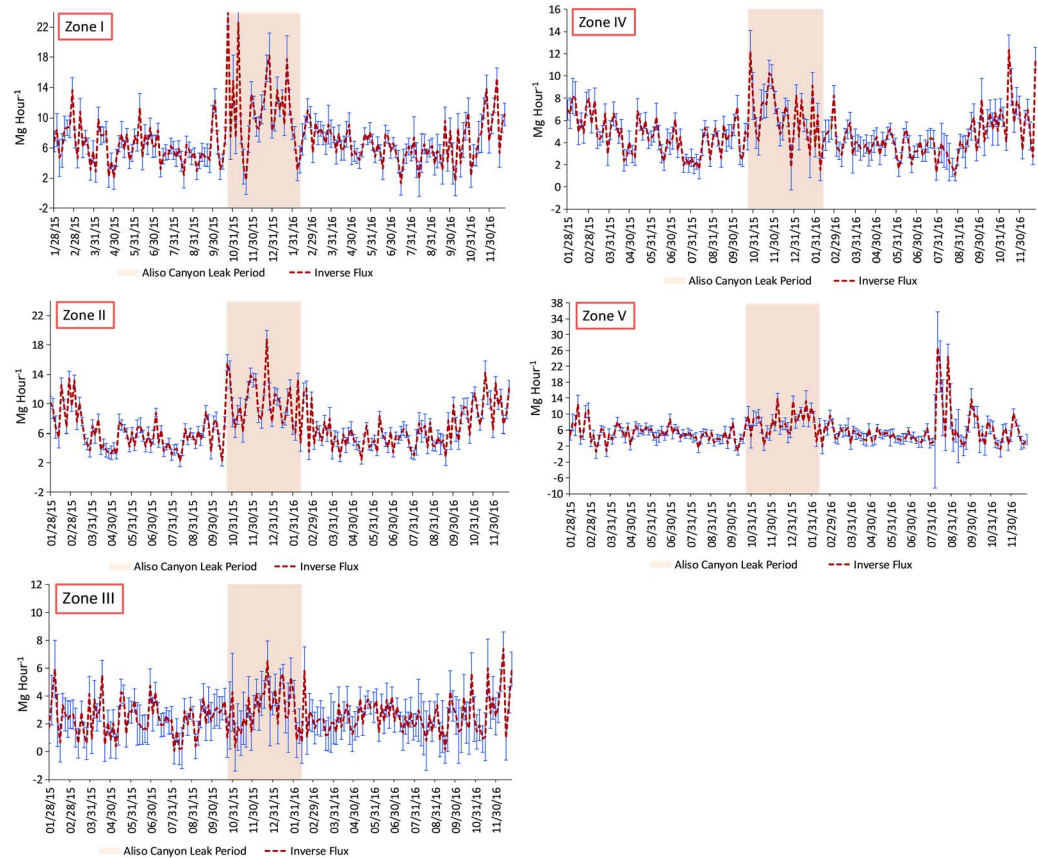


Figure 11. Time series of inverted CH₄ fluxes and estimated flux uncertainties for the five zones shown in Figure 1 from 28 January 2015 to 24 December 2016.

Spatially, it is extremely difficult to attribute the effect of Aliso Canyon to Zone I or Zone II as it is confounded by the density of the infrastructure, and regardless of the Aliso Canyon event, we have winter seasonal cycle of fluxes that is of similar magnitude as Aliso Canyon. Additionally, it is also important to note that on average residence time of air is approximately 12 hr in the basin (SoCAB); hence, computing fluxes at 4-day interval leads to spatiotemporal aggregation error. To avoid this error, large numbers of observations are required in comparison to what is available from eight towers and fluxes need be estimated at hourly interval. However, it is true that fluxes are larger in Zone I and Zone II in comparison to other zones, as can be confirmed by the density of CH₄-emitting infrastructure in Zone I and Zone II. Overall, we think that over long duration zonal estimates of fluxes as described here provides a true picture of the subbasin differences in the magnitude of fluxes.

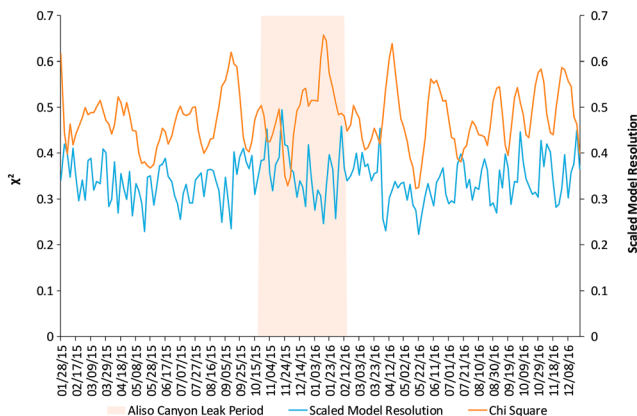


Figure 12. Time series of chi square and scaled model resolution for inverted fluxes from 28 January 2015 to 24 December 2016.

5.5. Inversion Performance

Using traditional metrics, the performance of inversions was within conventionally acceptable limits. For example, the correlation ($\text{corr}(z, \widehat{HS})$), between measured and forward modeled enhancements, was greater than 0.8 for most 4-day time periods, and the RMSE ranged from 0.05 ppm in summer months to 0.10 to 0.15 ppm in winter months inclusive of the Aliso Canyon leak period (e.g., Figure 5b). Relatively large winter months RMSE coincided with periods of higher uncertainties on estimated fluxes, which itself was the result of increased variance in rising enhancements at all sites. This also led to increased variance and degradation of the relationship between sensitivity and enhancement.

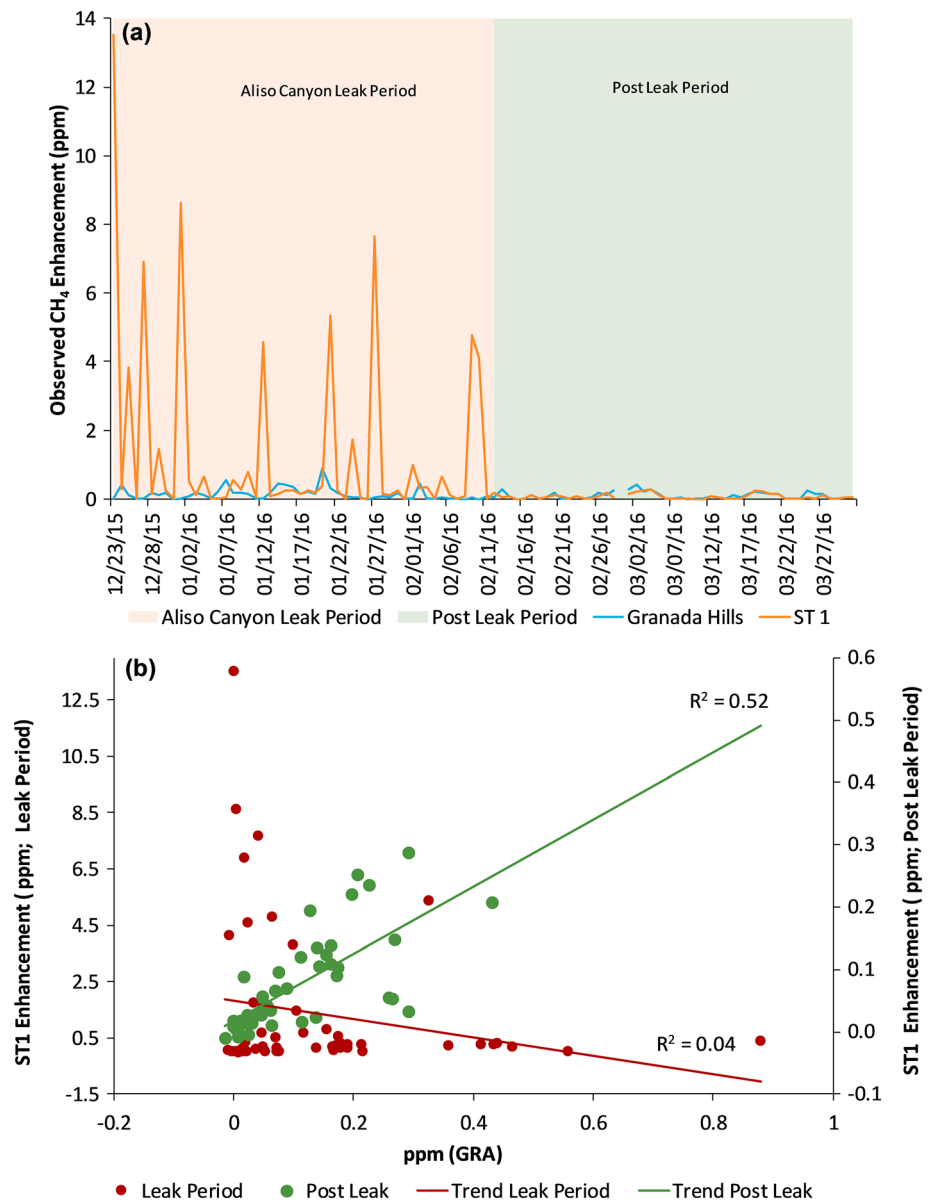


Figure 13. Time series of 1 p.m. daily CH₄ enhancement at Granada Hills (GRA) and ST1 in situ sites from 23 December 2015 to 31 March 2016. (b) The relationship between CH₄ enhancements at the two sites show in (a) during and after the Aliso Canyon leak.

The time series of $Tr(\hat{m})$, divided by the number of observations (scaled model resolution), which ranges from 0 to 1 and indicates the number of parameters (or fluxes) uniquely resolved by inversions, was between 0.25 and 0.40 for all times (see Figure 12). The χ^2_{red} statistic that reflects proper specification of error covariance ranged from 0.4 to 0.6, which indicates overestimation of errors if it is <1 and underestimation of errors if it is >1.

5.5.1. Impact of the Loss of Sensitivity on Flux Estimates

The Aliso Canyon incident illustrates a key limitation in the observing system. Thus, episodic insensitivity of the in situ network and the localized Aliso Canyon leak meant that there were periods when the inversions did not accurately capture basin-scale or localized fluxes (Figure 5). For example, for the period extending from 24 to 31 October 2015, inversions captured the anomalous CH₄ flux signal from the leak onset, but in most of November 2015 the sensitivity of in situ sites to key parts of the basin was significantly reduced due to prevailing wind conditions, which reduced the magnitude of fluxes obtained from

inversions. These sudden dropouts were inconsistent with physical emission processes and likely resulted from a combination of (1) limitations in the ability of the in situ network to capture the anomalous CH₄ flux signal from an extremely localized source and (2) limitations in the skill of our WRF-STILT model to represent atmospheric transport in the SoCAB, a region of complex terrain under the full range of meteorological situations. We applied three criteria to filter out flux estimates when the network was only partially sensitive to the sources of emissions constrained by GRA tower in Figure 5a. Specifically, we consider posterior fluxes valid (blue triangles) for periods when GRA mean enhancements were >0.1 ppm, site sensitivity was >0.8 ppm/μmol·m⁻²·s⁻¹, and the goodness of fit (chi square; see Michalak et al., 2005, p. 2, for details) was >0.5.

Temporal completeness is a serious consideration for applying inversions for constraining emission trends and variability. Hence, the many dropouts merit scrutiny. For example, the Aliso Canyon test case offered the opportunity to compare midday (1300 local time) CH₄ enhancements at our previously established GRA tower site (situated 9 km east of Aliso Canyon, inlet 50 m above ground level) and a temporary site (henceforth ST1) that was installed in Porter Ranch to help inform local residents about the presence of gas plumes. ST1 was operational from 23 December 2015 to 31 March 2016 and situated at ground level about 4 km southeast and (due to terrain) nearly 400 m below the Aliso Canyon gas leak source in a region of complex terrain. During the leak period, ST1 observed hourly enhancements as large as 13 ppm that were considerably larger than those observed at GRA. After the leak was plugged on 12 February 2016, CH₄ enhancements at both sites showed similar enhancements (see Figure 13a). As expected, the correlation between enhancements observed at the two sites increased from R^2 of near 0 during the leak period to approximately 0.52 after the leak was plugged (see Figures 13a and 13b). While both sites were equipped with the same high-precision sensors, neither was well situated for continuous quantification of the Aliso Canyon leak rate. The GRA site was frequently insensitive to the highly localized gas plume from Aliso Canyon given the prevailing (typically northerly) winds in fall 2015. Meanwhile, the Aliso plume and the highly localized effects of the canyon terrain dominated the ST1 site. As a result, WRF-STILT was not able to accurately represent atmospheric transport for both sites and particularly ST1. This resulted in poor correlation between sensitivity and enhancement at ST1, thereby preventing us from including this site in inversions. The utility of GRA was limited to when it and the rest of the measurement network were sensitive to the basin-wide flux including the contribution of the Aliso Canyon leak.

6. Conclusions

We examined the impact of the Aliso Canyon gas leak and the closure of the Puente Hills landfill on the evolution of CH₄ emissions in the SoCAB. The onset of the Aliso Canyon leak was captured by inversions that utilized tailored WRF-STILT meteorological output. However, sustained contribution of the leak to basin CH₄ emissions was not captured due to limited sensitivity of the network to the leak location (for details, see section 5.5.1). The closure of the Puente Hills landfill that represents a policy decision was captured in inversions, and we are not aware of any other regional inverse modeling study (not based on dedicated aircraft flights) that has accomplished this in an area with a dense CH₄-emanating infrastructure such as the SoCAB.

Spatially, the study for the first time utilized model resolution matrix to identify sources of major emissions in the basin. These sources were aligned with facilities identified in Vista-LA infrastructure inventory, giving us confidence that these locations are not artifacts of the inversion. Furthermore, the study significantly increased our understanding about the spatiotemporal variability of CH₄ fluxes in the SoCAB and key zones of the LA megacity domain by providing estimates of subbasin-scale fluxes.

The study also reaffirmed existing theories that a fraction of variability in enhancement and emissions in the basin is correlated with air temperature and energy demand. However, this has not been conclusively established in either this study or previous studies and would require detailed investigation, that is, studies that can isolate this process at the level of households (e.g., Fischer et al., 2018). Similarly, identification of the impact of episodic processes and apportioning of fluxes to specific facilities remained elusive due to the density and coverage provided by the current in situ network, indicating a requirement for a denser network, the establishment of which should be guided by pseudo data-inverse modeling studies that account for atmospheric transport (e.g., Pillai et al., 2012) in informing fluxes at an in situ site from near- and far-field sources.

Data Statement

Methane concentration data utilized in this study are already available from <https://megacities.jpl.nasa.gov/portal/>. These concentration data have also been submitted as part of the companion manuscript published in the *Journal of Geophysical Research: Atmospheres* and titled as “Detecting Urban Emissions Changes and Events with a Near-Real-Time-Capable Inversion System.” Output of Weather Research and Forecasting and Stochastic Time-Inverted Lagrangian Transport Model is ~ 50 TB in size, and researchers interested in obtaining these data should provide authors a data repository to upload the model output.

Acknowledgments

A portion of the research described in this paper was carried out at the Jet Propulsion Laboratory, California Institute of Technology, under contract with the National Aeronautics and Space Administration (NASA). Additional support was provided by the National Institute of Standards and Technology (NIST) Greenhouse Gas and Climate Science Measurements program. Measurements at SBC were supported by the California Air Resources Board project (11-306) at LBNL, operating under U.S. Department of Energy (DOE) contract DE-AC02-05CH11231. The authors also acknowledge support from NASA's Carbon Monitoring System program and the Prototype Methane Monitoring System for California project. Certain commercial equipment, instruments, or materials are identified in this paper in order to specify the experimental procedure adequately. Such identification is not intended to imply recommendation or endorsement by the National Institute of Standards and Technology, nor is it intended to imply that the materials or equipment identified are necessarily the best available for the purpose. The views expressed in this article are those of the authors and do not represent the views or policies of the California Air Resources Board.

References

- Andrae, R., Schulze-Hartung, T., & Melchior, P. (2010). Dos and don'ts of reduced chi-squared. *ArXiv:1012.3754 [Astro-Ph, Physics:Physics, Stat]*. Retrieved from <http://arxiv.org/abs/1012.3754>
- Aster, R. C., Borchers, B., & Thurber, C. H. (2018). *Parameter estimation and inverse problems*. Elsevier.
- CARB (2016). Aliso Canyon Methane Leak Climate Impacts Mitigation Program. Retrieved from https://ww3.arb.ca.gov/research/aliso_canyon/arb_aliso_canyon_methane_leak_climate_impacts_mitigation_program.pdf?_ga=2.250018182.1238799934.1556122700-1471337295.1550614786, Accessed on December 1st 2018, Sacramento, California.
- CARB (2018). Methane facility emissions study (p. https://www.arb.ca.gov/research/methane/facility_emissions_study_sa.xlsx?_ga=2.145167415.2090747175.1527610194-1075548182.1418233535). California Air Resources Board.
- Carranza, V., Rafiq, T., Frausto-Vicencio, I., Hopkins, F. M., Verhulst, K. R., Rao, P., et al. (2018). Vista-LA: Mapping methane-emitting infrastructure in the Los Angeles megacity. *Earth System Science Data*, 10(1), 653–676. <https://doi.org/10.5194/essd-10-653-2018>
- Chang, R. Y.-W., Miller, C. E., Dinardo, S. J., Karion, A., Sweeney, C., Daube, B. C., et al. (2014). Methane emissions from Alaska in 2012 from CARVE airborne observations. *Proceedings of the National Academy of Sciences*, 111(47), 16,694–16,699. <https://doi.org/10.1073/pnas.1412953111>
- Ciais, P., Sabine, C., Bala, G., Bopp, L., Brovkin, V., & House, J. I. (2014). Carbon and other biogeochemical cycles. In O. Edenhofer, et al. (Eds.), *Climate change 2013* (pp. 465–570). United Kingdom: Cambridge University Press.
- Conley, S., Franco, G., Faloona, I., Blake, D. R., Peischl, J., & Ryerson, T. B. (2016). Methane emissions from the 2015 Aliso Canyon blowout in Los Angeles, CA. *Science*, 351(6279), 1317–1320. <https://doi.org/10.1126/science.aaf2348>
- Cui, Y. Y., Brioude, J., McKeen, S. A., Angevine, W. M., Kim, S.-W., Frost, G. J., et al. (2015). Top-down estimate of methane emissions in California using a mesoscale inverse modeling technique: The South Coast Air Basin. *Journal of Geophysical Research: Atmospheres*, 120, 6698–6711. <https://doi.org/10.1002/2014JD023002>
- Department of Public Works (2018). Solid waste disposal summary reports by facilities (Los Angeles County). Los Angeles, California. Retrieved from <https://dpw.lacounty.gov/epd/swims/OnlineServices/reports.aspx>
- Dlugokencky, E. J., Bruhwiler, L., White, J. W. C., Emmons, L. K., Novelli, P. C., Montzka, S. A., et al. (2009). Observational constraints on recent increases in the atmospheric CH₄ burden. *Geophysical Research Letters*, 36, 18803. <https://doi.org/10.1029/2009GL039780>
- Duren, R. M., Thorpe, A., & Sander, S. P. (2017). California baseline methane survey: Interim phase 1 report. Sacramento, California: California Air Resources Board.
- Engelen, R. J., Denning, A. S., & Gurney, K. R. (2002). On error estimation in atmospheric CO₂ inversions. *Journal of Geophysical Research*, 107(D22), 4635. <https://doi.org/10.1029/2002JD002195>
- Fang, Y., Michalak, A. M., Shiga, Y. P., & Yadav, V. (2014). Using atmospheric observations to evaluate the spatiotemporal variability of CO₂ fluxes simulated by terrestrial biospheric models. *Biogeosciences*, 11, 6985–6997. <https://doi.org/10.5194/bg-11-6985-2014>
- Feng, S., Lauvaux, T., Newman, S., Rao, P., Ahmadvor, R., Deng, A., et al. (2016). Los Angeles megacity: A high-resolution land-atmosphere modelling system for urban CO₂ emissions. *Atmospheric Chemistry and Physics*, 16(14), 9019–9045. <https://doi.org/10.5194/acp-16-9019-2016>
- Fischer, M. L., Chan, W. R., Jeong, S., & Zhu, Z. (2018). *Natural gas methane emissions from California homes* (no. CEC-500-2018-021). Sacramento, California: California Energy Commission.
- Gourdji, S. M., Hirsch, A. I., Mueller, K. L., Yadav, V., Andrews, A. E., & Michalak, A. M. (2010). Regional-scale geostatistical inverse modeling of North American CO₂ fluxes: A synthetic data study. *Atmospheric Chemistry and Physics*, 10(13), 6151–6167. <https://doi.org/10.5194/acp-10-6151-2010>
- Gourdji, S. M., Mueller, K. L., Schaefer, K., & Michalak, A. M. (2008). Global monthly averaged CO₂ fluxes recovered using a geostatistical inverse modeling approach: 2. Results including auxiliary environmental data. *Journal of Geophysical Research*, 113, D21115. <https://doi.org/10.1029/2007JD009733>
- Henderson, J. M., Eluszkiewicz, J., Mountain, M. E., Nehrkorn, T., Chang, R. Y.-W., Karion, A., et al. (2015). Atmospheric transport simulations in support of the Carbon in Arctic Reservoirs Vulnerability Experiment (CARVE). *Atmospheric Chemistry and Physics*, 15(8), 4093–4116. <https://doi.org/10.5194/acp-15-4093-2015>
- Hopkins, F. M., Kort, E. A., Bush, S. E., Ehleringer, J. R., Lai, C.-T., Blake, D. R., & Randerson, J. T. (2016). Spatial patterns and source attribution of urban methane in the Los Angeles Basin. *Journal of Geophysical Research: Atmospheres*, 121, 2490–2507. <https://doi.org/10.1002/2015JD024429>
- Jeong, S., Newman, S., Zhang, J., Andrews, A. E., Bianco, L., Bagley, J., et al. (2016). Estimating methane emissions in California's urban and rural regions using multitower observations. *Journal of Geophysical Research: Atmospheres*, 121, 13,031–13,049. <https://doi.org/10.1002/2016JD025404>
- Jeong, S., Zhao, C., Andrews, A. E., Bianco, L., Wilczak, J. M., & Fischer, M. L. (2012). Seasonal variation of CH₄ emissions from central California. *Journal of Geophysical Research*, 117, D11306. <https://doi.org/10.1029/2011JD016896>
- Kirschke, S., Bousquet, P., Ciais, P., Saunoy, M., Canadell, J. G., Dlugokencky, E. J., et al. (2013). Three decades of global methane sources and sinks. *Nature Geoscience*, 6(10), 813–823. <https://doi.org/10.1038/ngo1955>
- Kitanidis, P. K. (1995). Quasi-linear geostatistical theory for inversing. *Water Resources Research*, 31(10), 2411–2419. <https://doi.org/10.1029/95WR01945>
- Kitanidis, P. K. (1996). On the geostatistical approach to the inverse problem. *Advances in Water Resources*, 19(6), 333–342. [https://doi.org/10.1016/0309-1708\(96\)00005-X](https://doi.org/10.1016/0309-1708(96)00005-X)

- Lin, J. C., Gerbig, C., Wofsy, S. C., Andrews, A. E., Daube, B. C., Davis, K. J., & Grainger, C. A. (2003). A near-field tool for simulating the upstream influence of atmospheric observations: The Stochastic Time-Inverted Lagrangian Transport (STILT) model. *Journal of Geophysical Research*, *108*(D16), 4493. <https://doi.org/10.1029/2002JD003161>
- Los Angeles County. (2016). Countywide integrated waste management plan. County of Los Angeles. Retrieved from <https://dpw.lacounty.gov/epd/swims/ShowDoc.aspx?id=6530&hp=yes&type=PDF>
- Maasackers, J. D., Jacob, D. J., Sulprizio, M. P., Turner, A. J., Weitz, M., Wirth, T., et al. (2016). Gridded national inventory of U.S. methane emissions. *Environmental Science & Technology*, *50*(23), 13,123–13,133. <https://doi.org/10.1021/acs.est.6b02878>
- Mann, H. B., & Whitney, D. R. (1947). On a test of whether one of two random variables is stochastically larger than the other. *The Annals of Mathematical Statistics*, 50–60.
- Michalak, A. M., Bruhwiler, L., & Tans, P. P. (2004). A geostatistical approach to surface flux estimation of atmospheric trace gases. *Journal of Geophysical Research*, *109*, D14109. <https://doi.org/10.1029/2003JD004422>
- Michalak, A. M., Hirsch, A., Bruhwiler, L., Gurney, K. R., Peters, W., & Tans, P. P. (2005). Maximum likelihood estimation of covariance parameters for Bayesian atmospheric trace gas surface flux inversions. *Journal of Geophysical Research*, *110*, D24.
- Miller, S. M., Michalak, A. M., & Levi, P. J. (2014). Atmospheric inverse modeling with known physical bounds: An example from trace gas emissions. *Geoscientific Model Development*, *7*(1), 303–315. <https://doi.org/10.5194/gmd-7-303-2014>
- Morris, V. R. (2016). *Ceilmeter Instrument Handbook* (No. DOE/SC-ARM-TR-020). DOE Office of Science Atmospheric Radiation Measurement (ARM) user facility (United States).
- Nehrkorn, T., Henderson, J., Mountain, M. E., Barrera, Y., Hegarty, J. D., Sargent, M. R., et al. (2018). Evaluation of recent WRF options for modeling atmospheric transport of greenhouse gases at regional and urban scales. AGU Fall Meeting Abstracts, 21. Retrieved from <http://adsabs.harvard.edu/abs/2018AGUFM.B21J2464N>
- Peischl, J., Ryerson, T. B., Brioude, J., Aikin, K. C., Andrews, A. E., Atlas, E., et al. (2013). Quantifying sources of methane using light alkanes in the Los Angeles basin, California. *Journal of Geophysical Research: Atmospheres*, *118*, 4974–4990. <https://doi.org/10.1002/jgrd.50413>
- Pillai, D., Gerbig, C., Kretschmer, R., Beck, V., Karstens, U., Neining, B., & Heimann, M. (2012). Comparing Lagrangian and Eulerian models for CO₂ transport—a step towards Bayesian inverse modeling using WRF/STILT-VPRM. *Atmospheric Chemistry and Physics*, *12*(19), 8979–8991.
- Santoni, G. W., Daube, B. C., Kort, E. A., Jiménez, R., Park, S., Pittman, J. V., et al. (2014). Evaluation of the airborne quantum cascade laser spectrometer (QCLS) measurements of the carbon and greenhouse gas suite—CO₂, CH₄, N₂O, and CO—during the CalNex and HIPPO campaigns. *Atmospheric Measurement Techniques*, *7*(6), 1509–1526. <https://doi.org/10.5194/amt-7-1509-2014>
- Shiga, Y. P., Michalak, A. M., Gourdji, S. M., Mueller, K. L., & Yadav, V. (2014). Detecting fossil fuel emissions patterns from subcontinental regions using North American in situ CO₂ measurements. *Geophysical Research Letters*, *41*, 4381–4388.
- Spokas, K., Bogner, J., Corcoran, M., & Walker, S. (2015). From California dreaming to California data: Challenging historic models for landfill CH₄ emissions. *Earth & Environmental Science*, *3*, 000051. <http://doi.org/10.12952/journal.elementa.000051>
- Spokas, K. A., & Bogner, J. E. (2011). Limits and dynamics of methane oxidation in landfill cover soils. *Waste Management*, *31*(5), 823–832.
- Tarantola, A. (2004). *Inverse problem theory and methods for model parameter estimation* (1st ed.). Philadelphia, PA: SIAM: Society for Industrial and Applied Mathematics.
- Thoning, K. W., Tans, P. P., & Komhyr, W. D. (1989). Atmospheric carbon dioxide at Mauna Loa Observatory: 2. Analysis of the NOAA GMCC data, 1974–1985. *Journal of Geophysical Research*, *94*(D6), 8549–8565.
- Verhulst, K. R., Karion, A., Kim, J., Salameh, P. K., Keeling, R. F., Newman, S., et al. (2017). Carbon dioxide and methane measurements from the Los Angeles megacity carbon project—Part 1: Calibration, urban enhancements, and uncertainty estimates. *Atmospheric Chemistry and Physics*, *17*(13), 8313–8341. <https://doi.org/10.5194/acp-17-8313-2017>
- Ware, J., Kort, E. A., Duren, R., Mueller, K. L., Verhulst, K., & Yadav, V. (2019). Detecting urban emissions changes and events with a near-real-time-capable inversion system. *Journal of Geophysical Research: Atmospheres*, *124*. <https://doi.org/10.1029/2018JD029224>
- Wecht, K. J., Jacob, D. J., Sulprizio, M. P., Santoni, G. W., Wofsy, S. C., Parker, R., et al. (2014). Spatially resolving methane emissions in California: Constraints from the CalNex aircraft campaign and from present (GOSAT, TES) and future (TROPOMI, geostationary) satellite observations. *Atmospheric Chemistry and Physics*, *14*(15), 8173–8184. <https://doi.org/10.5194/acp-14-8173-2014>
- Wennberg, P. O., Mui, W., Wunch, D., Kort, E. A., Blake, D. R., Atlas, E. L., et al. (2012). On the sources of methane to the Los Angeles atmosphere. *Environmental Science & Technology*, *46*(17), 9282–9289. <https://doi.org/10.1021/es301138y>
- Wong, C. K., Pongetti, T. J., Oda, T., Rao, P., Gurney, K. R., Newman, S., et al. (2016). Monthly trends of methane emissions in Los Angeles from 2011 to 2015 inferred by CLARS-FTS observations. *Atmospheric Chemistry and Physics*, *16*(20), 13,121–13,130. <https://doi.org/10.5194/acp-16-13121-2016>
- Wunch, D., Toon, G. C., Hedelius, J. K., Vizenor, N., Roehl, C. M., Saad, K. M., et al. (2016). Quantifying the loss of processed natural gas within California's South Coast Air Basin using long-term measurements of ethane and methane. *Atmospheric Chemistry and Physics*, *16*(22), 14,091–14,105. <https://doi.org/10.5194/acp-16-14091-2016>
- Wunch, D., Wennberg, P. O., Toon, G. C., Keppel-Aleks, G., & Yavin, Y. G. (2009). Emissions of greenhouse gases from a North American megacity. *Geophysical Research Letters*, *36*, L15810. <https://doi.org/10.1029/2009GL039825>
- Yadav, V., Michalak, A. M., Ray, J., & Shiga, Y. P. (2016). A statistical approach for isolating fossil fuel emissions in atmospheric inverse problems. *Journal of Geophysical Research: Atmospheres*, *121*, 12,490–12,504. <https://doi.org/10.1002/2016JD025642>